Electronic Supplementary Information

Hierarchical CoMoP/NiCoP Heterostructures on Nickel Foam for Efficient Electrochemical Nitrate-to-Ammonia Conversion at Industrial Current Densities

Min Xu,[a,b] Shengbo Zhang,[a,b] Hui Xu,*[a,b] Zhixian Mao,[a,b] Zenglong Wu,[a,b] Huajie Yin,[a,b] and Haimin Zhang*[a,b]

[a] Key Laboratory of Materials Physics, Centre for Resource Innovation, Anhui Key Laboratory of Nanomaterials and Nanotechnology, Institute of Solid State Physics, HFIPS, Chinese Academy of Sciences, Hefei 230031, Anhui, China.

[b] University of Science and Technology of China, Hefei 230026, Anhui, China.

* Corresponding author: E-mail: hxu@issp.ac.cn, zhanghm@issp.ac.cn.

1. Experimental section

1.1 Chemicals and materials

Cobalt(II) nitrate hexahydrate ($Co(NO_3)_2 \cdot 6H_2O$, AR, ≥99%), Sodium molybdate dihydrate ($Na_2MoO_4 \cdot 2H_2O$, AR, ≥99%), Urea ($CO(NH_2)_2$, AR, ≥99%), Sodium hypophosphite monohydrate ($NaH_2PO_2 \cdot H_2O$), Sodium nitroferricyanide dihydrate ($Na_2[(Fe(CN)_5NO)] \cdot 2H_2O$, AR, ≥99%), Sodium salicylate ($C_7H_5NaO_3$, ≥99%), Sodium citrate ($C_6H_5O_7Na_3$, ≥98%), Sulfanilamide ($C_6H_8N_2O_2S$, AR, ≥99%), N-(1-naphthyl) ethylenediamine dihydrochloride ($C_{12}H_{14}N_2 \cdot 2HCl$, AR, ≥98%) were purchased from Aladdin Reagent Company. NaClO (AR, 6-14% active chlorine base), NH_4Cl (AR, ≥99.5%), $NaNO_2$ (AR, ≥99%) were purchased from Shanghai Aladdin Bio-Chem Technology Co., Ltd. NaOH (AR, ≥96%), KOH (AR, ≥85.0%) were purchased from Sinopharm Chemical Reagent Co., Ltd. Deionized water (DW) made by laboratory. All chemicals were used without further purification.

1.2 Catalyst Synthesis

Synthesis of NiCoO/NF: In a typical synthesis, $Co(NO)_3 \cdot 6H_2O$ (2 mmol) and urea (10 mmol) were dissolved in 35 mL water under vigorous stirring for 30 min. Then the solution was transferred into a 80 mL Teflon-lined stainless autoclave. Immerse a cleaned nickel foam (3×3 cm) into the reaction solution, seal the autoclave, and react at 120 °C for 6 hours. After the autoclave cooled down slowly at room temperature, After allowing the autoclave to cool slowly to room temperature, the NiCoO/NF was taken out, and washed thoroughly with water and ethanol.

Synthesis of $CoMoO_4$/NiCoO/NF: $Na_2MoO_4 \cdot 2H_2O$ (2mmol) was dissolved in 35 mL

water under vigorous stirring for 30 min. Then the solution was transferred into a 80 mL Teflon-lined stainless autoclave. A piece of NiCoO/NF was immersed in the solution. The autoclave was sealed and maintained at 130 °C for 6 h. After the autoclave cooled down slowly at room temperature, the $CoMoO_4$/NiCoO/NF was taken out and washed with water and ethanol thoroughly before vacuum dried.

Synthesis of CoMoP/NiCoP/NF: To syntheize CoMoP/NiCoP/NF, Two porcelain boats containing $NaH_2PO_2 \cdot H_2O$ (1 g) and $CoMoO_4$/NiCoO/NF were placed upstream and downstream in the tube furnace, respectively. Subsequently, the samples were heated at 300 °C with 1°C min^{-1} and kept for 2 h at the Ar atmosphere, and then naturally cooled to room temperature.

Synthesis of NiCoP/NF: To syntheize NiCoP/NF, Two porcelain boats containing $NaH_2PO_2 \cdot H_2O$ (1 g) and NiCoO/NF were placed upstream and downstream in the tube furnace, respectively. Subsequently, the samples were heated at 300 °C with 1°C min^{-1} and kept for 2 h at the Ar atmosphere, and then naturally cooled to room temperature.

1.3 Material Characterization

The crystalline structure of the samples were characterized using a Philips X'pert Pro X-ray diffractometer with Cu Kα radiation (Kα = 0.15418 nm) operated at 40 kV and 40 mA. Scanning electron microscopy (SEM) images were acquired on an SU8020 field-emission microscope (Hitachi, Japan) at an accelerating voltage of 10.0 kV. Transmission electron microscopy (TEM) was conducted on Tecnai G2 F20 instrument at 200 kV. X-ray photoelectron spectroscopy (XPS) measurements were performed on ESCALAB 250 spectrometer (Thermo Scientific, USA) with monochromated Al Kα

X-ray source (1486.6 eV). Raman spectra were recorded on a Renishaw in Via confocal Raman microscope with a 532 nm laser source and a 50X objective lens. UV-Vis absorption spectra were obtained using SHIMADZU UV-2700 spectrophotometer. Electron spin resonance (ESR) spectra were collected on a Bruker EMXplus 10/12 spectrometer equipped with an Oxford ESR910 liquid helium cryostat. ^{1}H nuclear magnetic resonance (^{1}H NMR) spectra were recorded on Bruker Ascend™ 400 MHz spectrometer.

1.4 Electrochemical measurements

All electrochemical measurements were conducted on a DH7002 electrochemical workstation (Jiangsu Donghua Analytical Instrument Co., Ltd.) using a three-electrode H-type cell configuration. Electrodes were separated by a Nafion® 211 membrane, and the working electrode was CoMoP/NiCoP/NF (1×0.4 cm^2). Current density was defined based on an effective area of 1 cm^2. (scaled current data). A saturated Hg/HgO electrode and a platinum mesh were employed as the reference electrode and counter electrode, respectively. All electrochemical measurements were carried out under continuous magnetic stirring at a constant speed of 500 rpm to ensure sufficient mass transport and minimize concentration polarization, especially at high current densities. Linear sweep voltammetry (LSV) was performed at a fixed scan rate of 10 mV s^{-1}. All potentials measured against the Hg/HgO reference were converted to the reversible hydrogen electrode (RHE) scale using the following equation:

$$E_{(RHE)} = E_{(Hg/HgO)} + 0.098 + 0.059 \times pH$$

1.5 Determination of ammonia

The concentration of electrochemically produced ammonia was quantified using the indophenol blue method. The colorimetric reagents were prepared as follows: Color Reagent A was obtained by dissolving 10 g of salicylic acid and 10 g of sodium citrate in 55 mL of 2 M NaOH solution, followed by dilution to 200 mL with deionized water. Oxidizing Reagent B was prepared by mixing 5 mL of sodium hypochlorite solution with 45 mL of 2 M NaOH solution. Reagent C was made by dissolving 1.0 g of $Na_2[Fe(CN)_5NO]\cdot 2H_2O$ in deionized water and diluting to a final volume of 100 mL. After electrolysis, the electrolyte was appropriately diluted. Then, 10 mL of the diluted solution was transferred to a colorimetric tube, followed by sequential addition of 500 μL of Reagent A, 100 μL of Reagent B, and 100 μL of Reagent C. After thorough mixing, the solution was allowed to develop color at room temperature for 1 hour. The absorbance was measured at a wavelength of 697.5 nm using a UV-Vis spectrophotometer. The ammonia concentration was determined based on a pre-established calibration curve.

1.6 Determination NO_2^-

The concentration of nitrite (NO_2^-) generated was determined by the Griess reagent method. The colorimetric agent was prepared as follows: 50 mL of phosphoric acid was diluted in 250 mL of deionized water, followed by dissolving 20 g of sulfanilamide and 1 g of N-(1-naphthyl)ethylenediamine dihydrochloride in the resulting solution. The mixture was then transferred to a 500 mL volumetric flask and brought to the mark with deionized water. After the electrochemical test, the electrolyte was diluted appropriately. Then, 10 mL of the diluted solution was placed in a 10 mL colorimetric

tube, and 200 μL of the Griess reagent was added. After thorough mixing, the solution was allowed to develop color at room temperature for 20 minutes. The absorbance was measured at 540 nm using a UV-Vis spectrophotometer. The nitrite concentration was calculated based on a pre-established calibration curve.

1.7 Calculation of NtrRR Performance

The yield of NH_3 (R_{NH3}), Faradaic efficiency (FE), and S_{NH3} were calculated according to the following equations:

$$R_{NH_3}(mg\ h^{-1}\ cm^{-2}) = \frac{C_{NH_3}(mg\ mL^{-1}) \times V(mL)}{t(h) \times m(mg)}$$

$$FE(\%) = \frac{8 \times n_{NH_3}(mol) \times F(mol^{-1})}{Q(C)}$$

where C_{NH3} denotes the concentration of produced ammonia, V represents the volume of the electrolyte, t is the electrolysis time, and m is the mass of the loaded electrocatalyst. F is the Faraday constant (96485 C mol^{-1}), and Q is the total charge transferred during electrolysis. C_{NH3}-N and C_{NO2^-}-N correspond to the concentrations of nitrogen in the form of NH_3 and NO_2^-, respectively.

The yield of NO_2^- (R_{NO2^-}) and Faradaic efficiency (FE) were calculated according to the following equations:

$$R_{NO_2-}(mg\ h^{-1}\ cm^{-2}) = \frac{C_{NO_2-}(mg\ mL^{-1}) \times V(mL)}{t(h) \times m(mg)}$$

$$FE(\%) = \frac{2 \times n_{NH_3}(mol) \times F(mol^{-1})}{Q(C)}$$

$C_{NO2-}$is the measured NO_2^- concentration and V is the volume of electrolyte solution. t is the electrolysis time, m is the mass of the loaded electrocatalyst, F is the faradaic

constant (96485 C mol^{-1}) and Q is the total charge transferred during electrolysis.

1.8 ^{15}N Isotope Labeling Experiments

^{15}N isotopic labeling experiments were conducted using $K^{15}NO_3$ as the sole nitrogen source, following the same procedure as that with KNO_3. After the test, the electrolyte was first acidified with dilute H_2SO_4 to adjust the pH to approximately 3~4. The acidified solution was then analyzed by ^1H NMR spectroscopy using a Bruker Avance 400 MHz spectrometer.

1.9 ESR measurements

Using 5,5-Dimethyl-1-Pyrroline-N-oxide (DMPO) as a spin-trapping agent (with a final concentration of 2~5 mM in the detection system), hydrogen radicals (*H) were detected by electron paramagnetic resonance (EPR) spectroscopy. Specifically, 200 μL of DMPO was added to 10 mL of the electrolyte. After 5 min of potentiostatic electrolysis, 1 mL of the mixture was collected and transferred into a capillary tube for EPR measurement.

1.10 Electrochemical online DEMS measurements

Online electrochemical differential electrochemical mass spectrometry (DEMS) measurements were carried out in a custom-designed electrochemical cell. The electrolyte consisted of a 0.1 M KNO_3 and 1.0 M KOH aqueous solution. a piece of CoMoP/NiCoP/NF (1.0 × 0.5 cm) electrocatalyst was used as the working electrode, while a platinum wire and an Hg/HgO electrode served as the counter and reference electrodes, respectively. Electrocatalysis was performed potentiostatically at -0.4 V (*vs.* RHE) in alternating periods. After each electrocatalytic interval, the system was

allowed to stabilize until the mass spectrometry signal returned to the baseline before commencing the next cycle. The experiment was terminated after 4 complete cycles.

1.11 Electrochemical in-situ FTIR measurements

Electrochemical in-situ FTIR spectroscopy were performed on a FTIR spectrometer (Nicolet iS50, Thermo Scientific) equipped with an MCT-A detector and a silicon prism window. First, a piece of CoMoP/NiCoP/NF (0.5 × 0.5 cm) was cut and flattened on a tablet press to serve as the working electrode. A platinum mesh electrode and an Hg/HgO electrode served as the counter and reference electrodes, respectively. The electrolyte used was 1.0 M KOH solution containing 0.1 M KNO_3. Each infrared absorption spectrum was obtained by averaging 128 scans at a resolution of 4.0 cm^{-1}. Prior to each measurement, a background spectrum of the catalyst electrode was collected at open-circuit potential. The measurements were performed within a potential range from 0 V to -0.8 V (*vs.* RHE), with increments of 0.1 V.

1.12 Energy consumption analysis

The relevant Energy consumptions (E_{spec}) was calculated according to the following equations:

$$V_{cell}(V) \approx |E(vs.\,RHE)| + V_{OER}$$

In 1 M KOH, V_{OER} is typically taken as ~1.5 V. This value incorporates the equilibrium potential of OER (~1.23 V), the typical overpotential (~0.3-0.5 V), and partial ohmic losses.[1]

$$E_{spec}(kWh\,kg^{-1}) = \frac{Q(C) \times V_{cell}(V)}{m_{NH3}(kg) \times 3.6 \times 10^{6}}$$

where Q is the total charge transferred during electrolysis V_{cell} is the cell voltage (V).

and m_{NH3} is the total mass of ammonia.

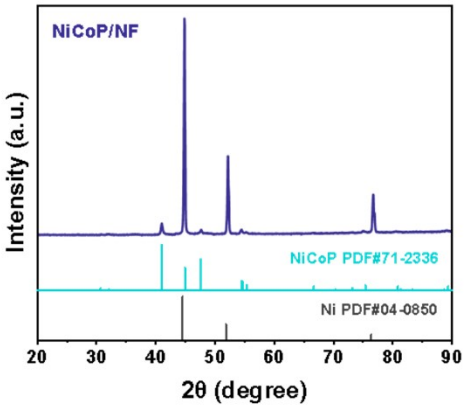

Fig. S1 XRD patterns of pristine NiCoP/NF.

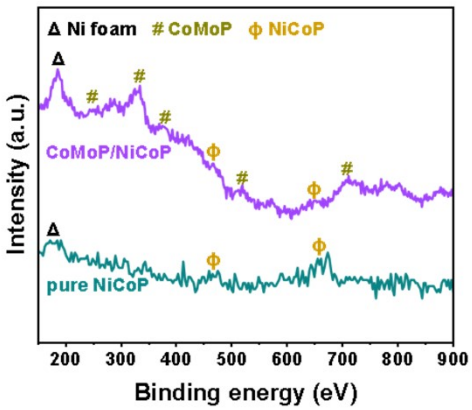

Fig. S2 The high-resolution Raman spectra for CoMoP/NiCoP and pure-CoMoP on the Ni foam.

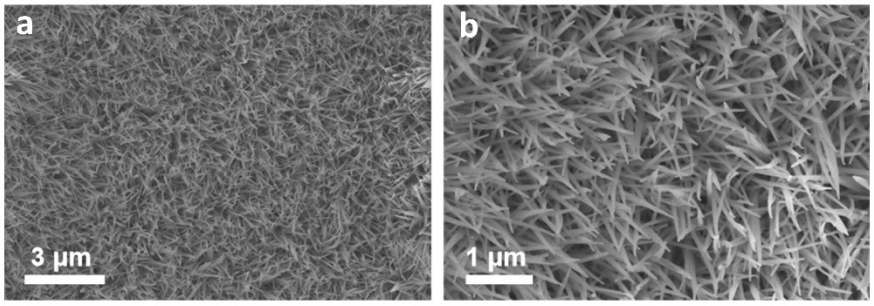

Fig. S3. SEM image of (a) NiCoO/NF and (b) NiCoP/NF.

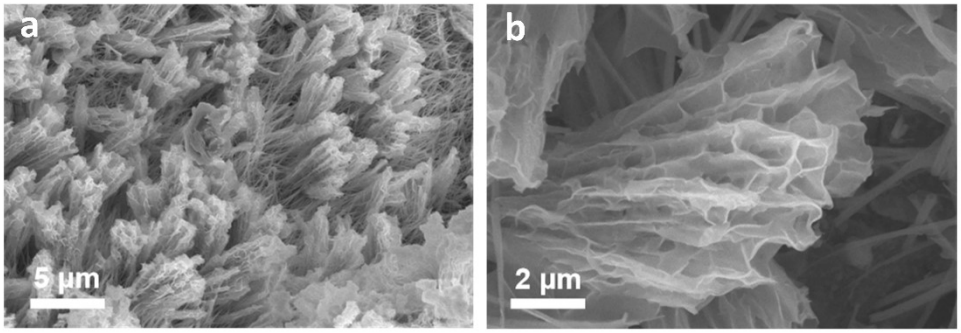

Fig. S4 SEM image of CoMoO/NiCoO/NF.

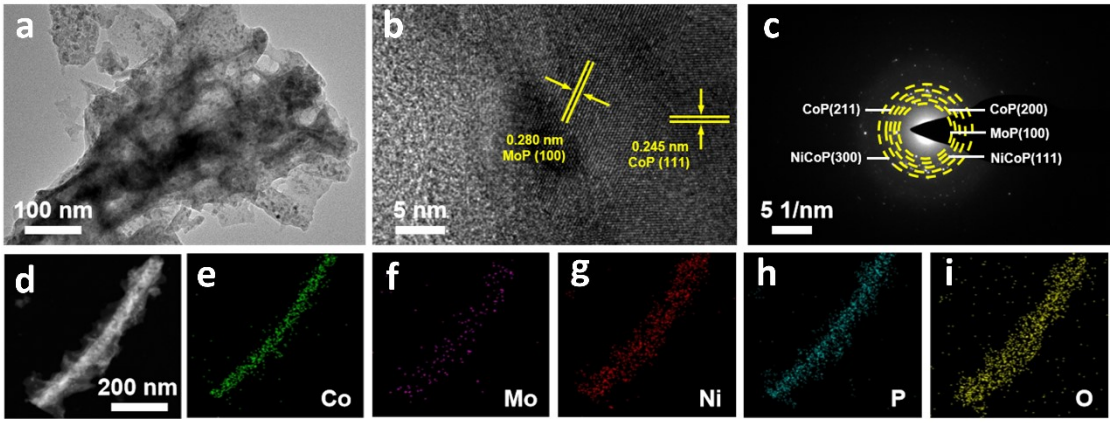

Fig. S5 (a) Low-magnification TEM image, (b) High-resolution TEM image and (c) the corresponding FFT image of CoMoP/NiCoP/NF. (d-i) HAADF-STEM image and corresponding element mappings of CoMoP/NiCoP/NF.

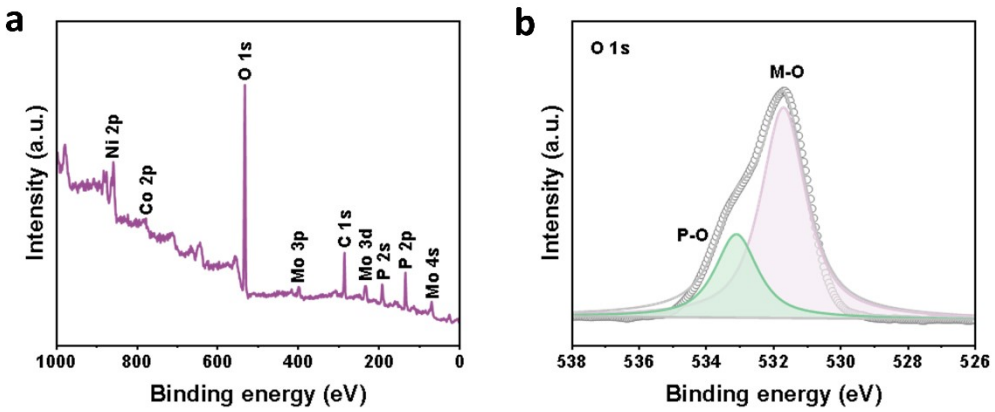

Fig. S6(a) Surface survey XPS spectrum and high-resolution (b) O 1s XPS spectra of CoMoP/NiCoP/NF.

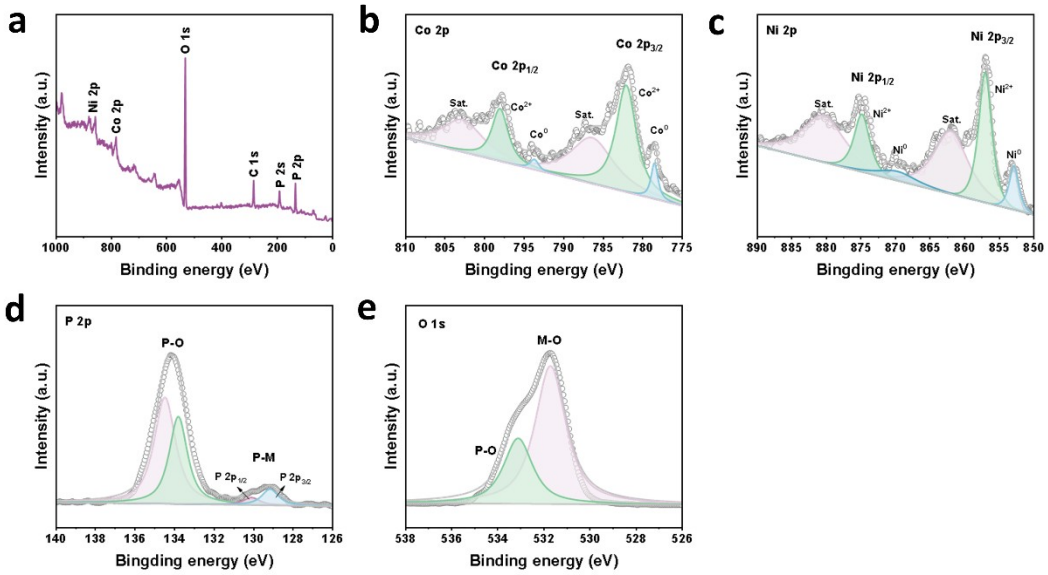

Fig. S7 (a) Surface survey XPS spectrum and high-resolution (b) Co 2p, (c) Ni 2p, (d) P 2p and (e) O 1s XPS spectra of NiCoP/NF.

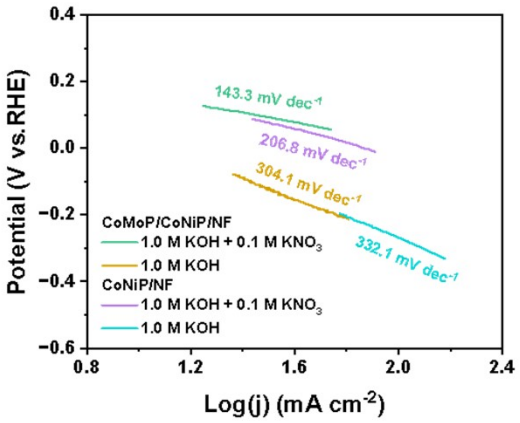

Fig. S8 The Tafel slope of LSV for eNO_3^-RR on CoMoP/NiCoP/NF and NiCoP/NF.

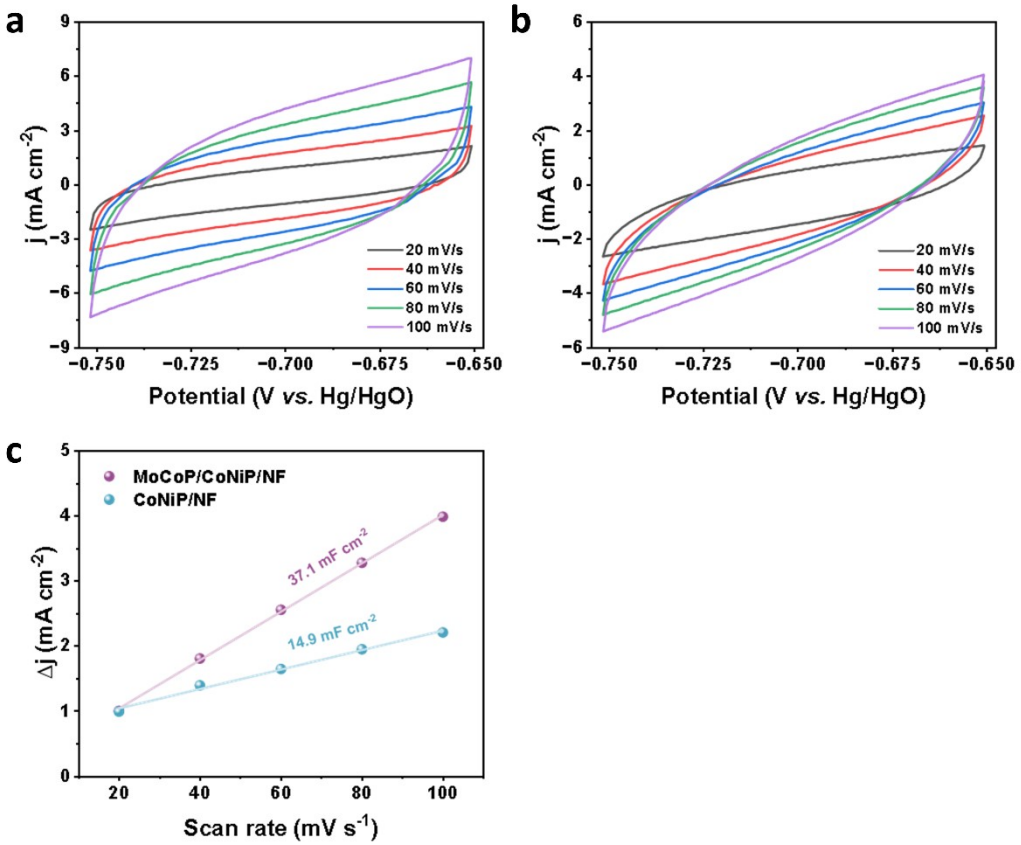

Fig. S9 The cyclic voltammetry curves of (a) CoMoP/NiCoP/NF and (b) NiCoP/NF with various scan rates (20, 40, 60, 80, 100 mV s^{-1}) in the region of -0.75 V to -0.85 V (vs. Hg/HgO). (c) The capacitive current densities at 0.22 V (vs. Hg/HgO) as a function of scan rates for different catalysts.

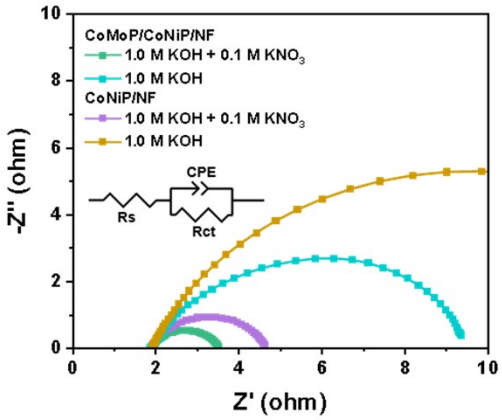

Fig. S10 The electrochemical impedance spectra of CoMoP/NiCoP/NF and NiCoP/NF under different conditions.

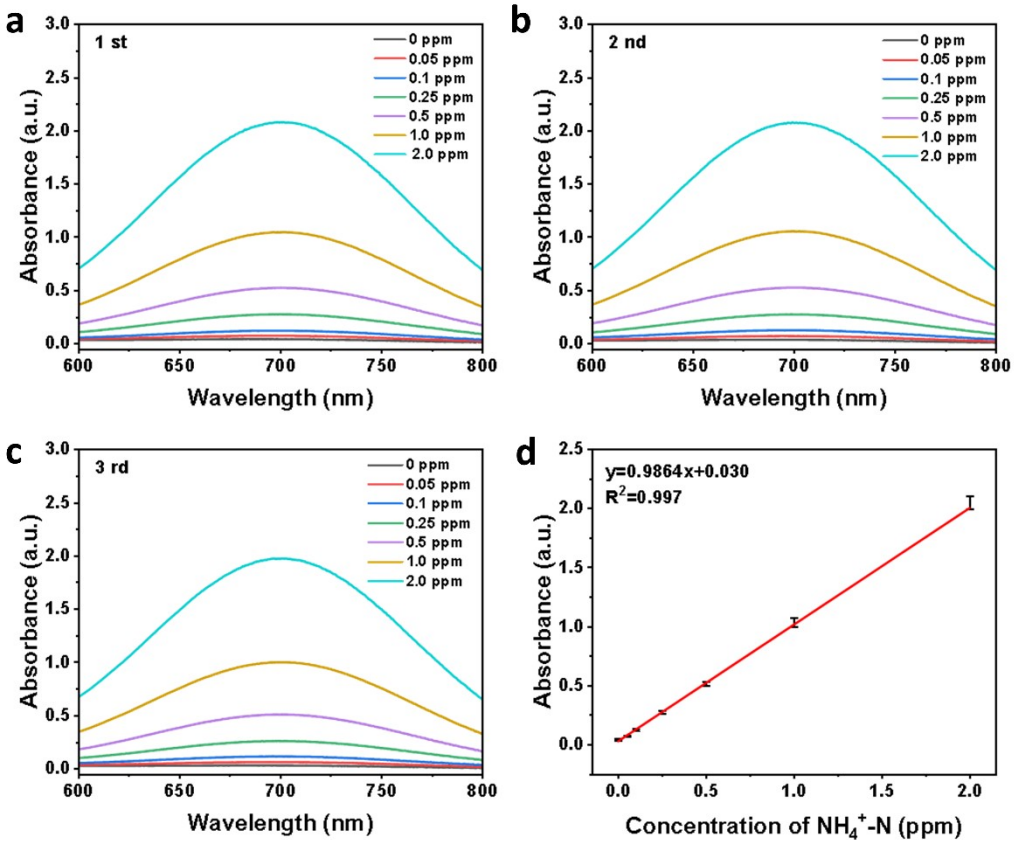

Fig. S11 (a-c) UV-Vis spectra of various NH_4^+-N concentrations for three repeated experiments. (d) The calibration curve used for calculation of NH_4^+-N concentration.

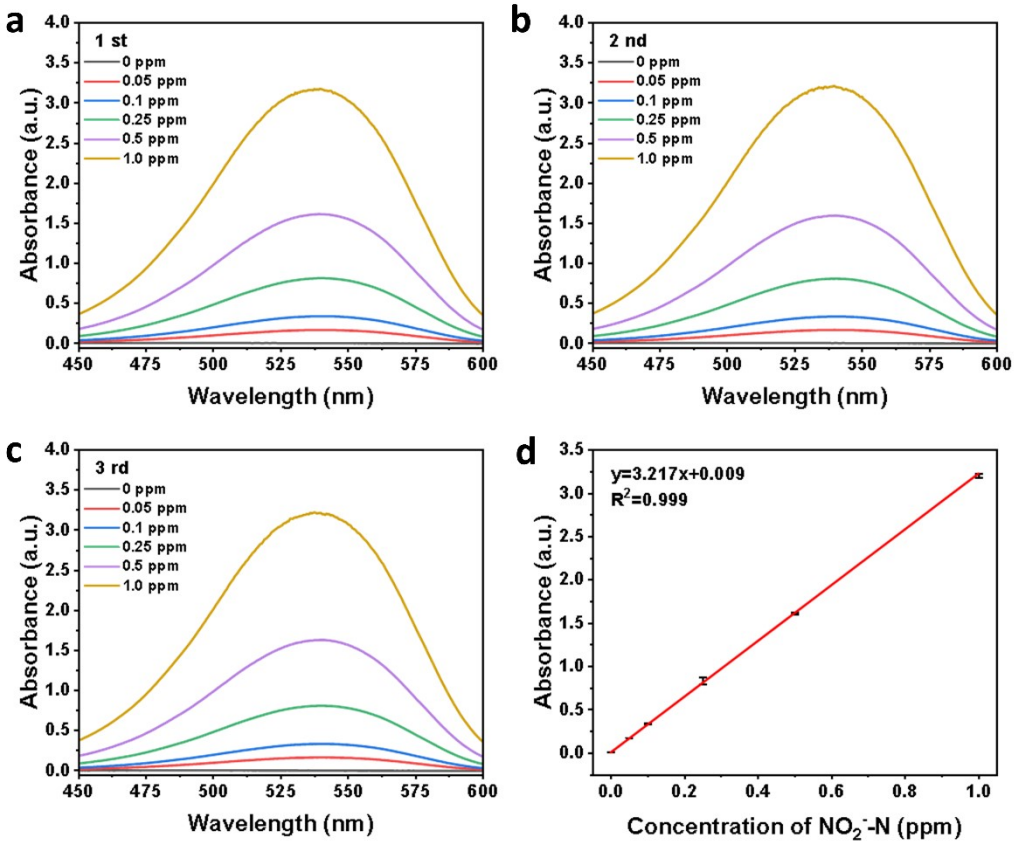

Fig. S12 (a-c) UV-Vis spectra of various NO_2^--N concentrations for three repeated experiments. (d) The calibration curve used for calculation of NO_2^--N concentration.

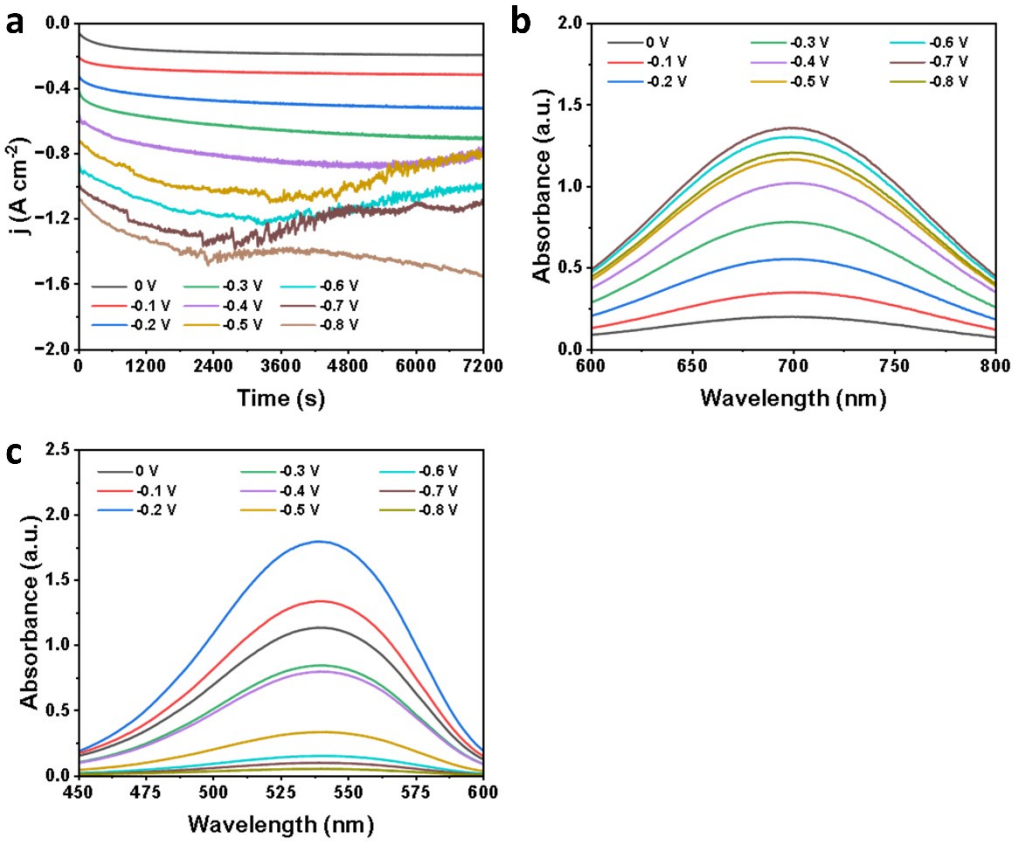

Fig. S13 (a) The chronoamperometric curves of CoMoP/NiCoP/NF at different potentials in 1.0 M KOH + 0.1 M KNO_3 electrolyte over a 2 h period. UV-Vis spectra of (b) NH_4^+-N and (c) NO_2^--N for the corresponding samples.

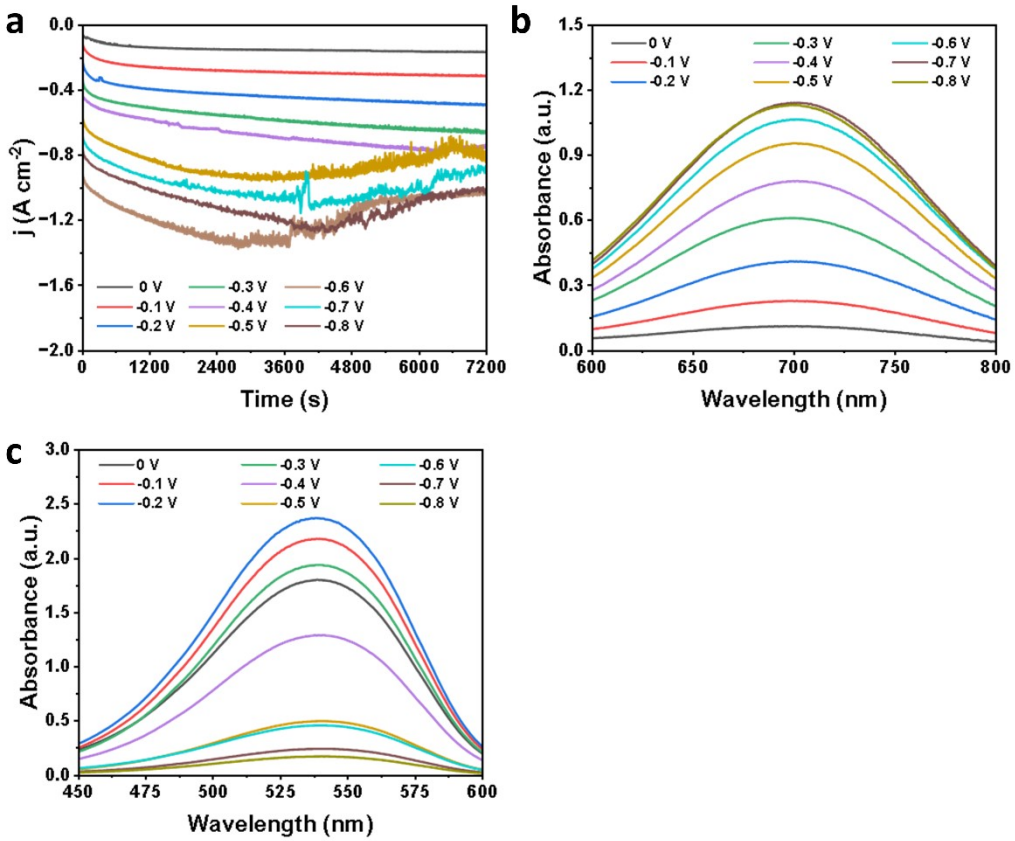

Fig. S14 (a) The chronoamperometric curves of NiCoP/NF at different potentials in 1.0 M KOH + 0.1 M KNO_3 electrolyte over a 2 h period. UV-Vis spectra of (b) NH_4^+-N and (c) NO_2^--N for the corresponding samples.

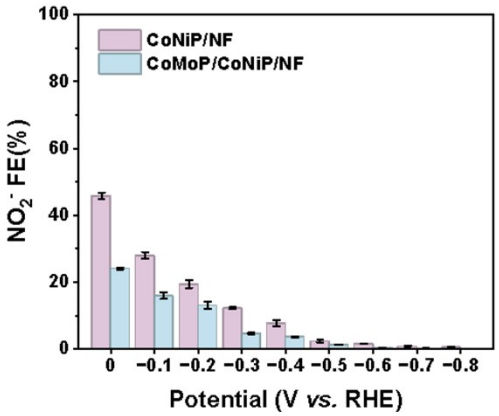

Fig. S15 NO_2^- FE of CoMoP/NiCoP/NF and NiCoP/NF at different applied potentials in 1.0 M KOH + 0.1 M KNO_3 electrolyte over a 2 h period.

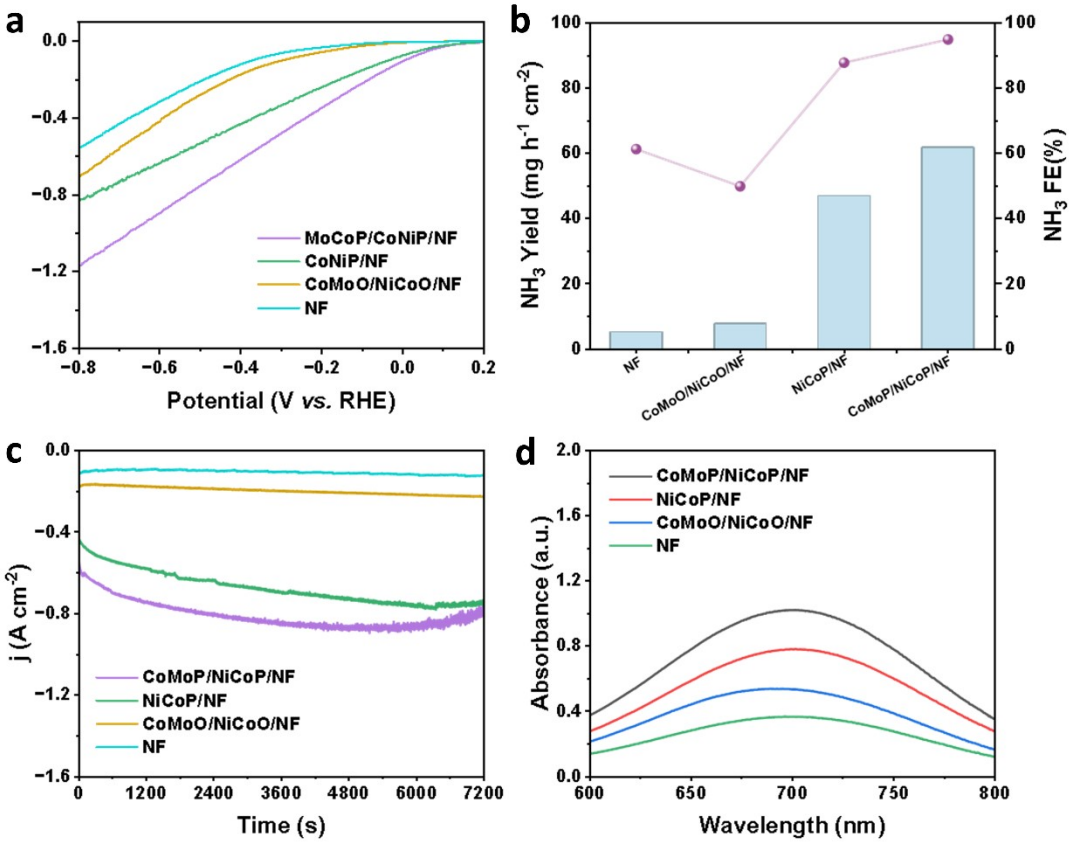

Fig. S16 (a) LSV curves in 1 M KOH with 0.1 M KNO_3. (b) NH_3 yield rate and FE of different catalyst at -0.4 V (*vs.* RHE). (c) The chronoamperometric curves of different catalyst at -0.4 V (*vs.* RHE) over a 2 h period. (d)UV-Vis spectra of NH_4^+-N for the corresponding samples.

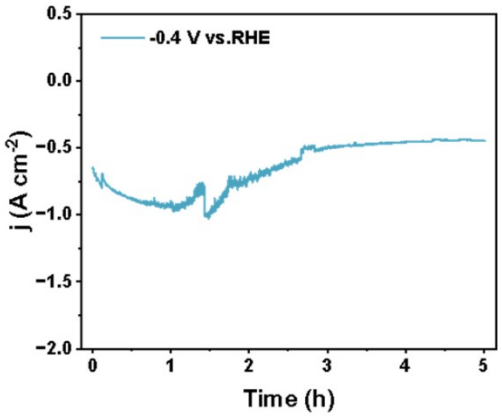

Fig. S17 The chronoamperometric curves of CoMoP/NiCoP/NF at -0.4 V (*vs.* RHE) over a 5 h period.

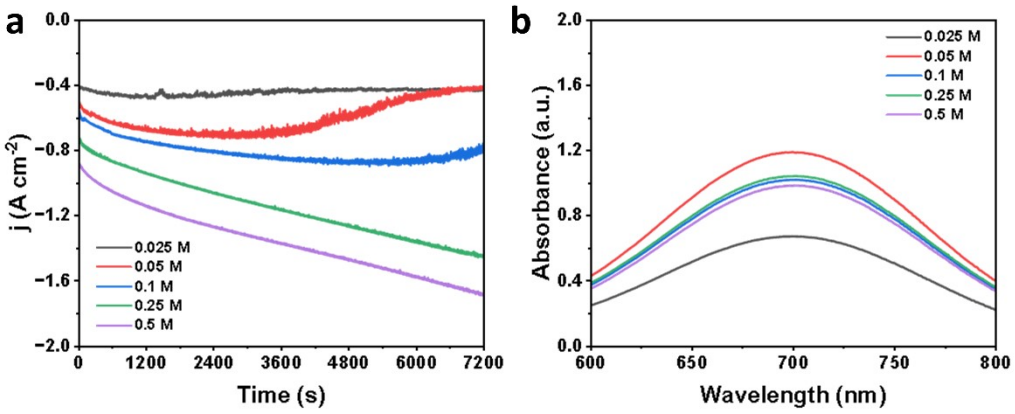

Fig. S18 (a) The chronoamperometric curves of CoMoP/NiCoP/NF at -0.4 V (*vs.* RHE) in different concentrations over a 2 h period. (b) UV-Vis spectra of NH_4^+-N for the corresponding samples.

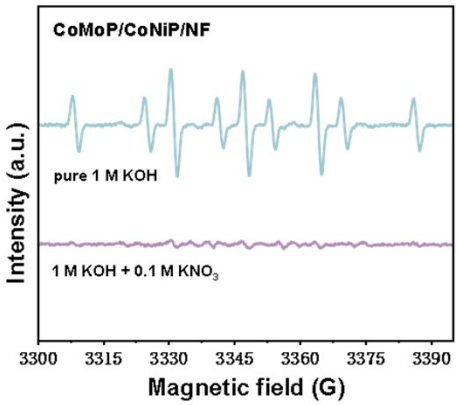

Fig. S19 DMPO-involved electron spin resonance (ESR) spectra of CoMoP/NiCoP/NF under different electrolysis conditions.

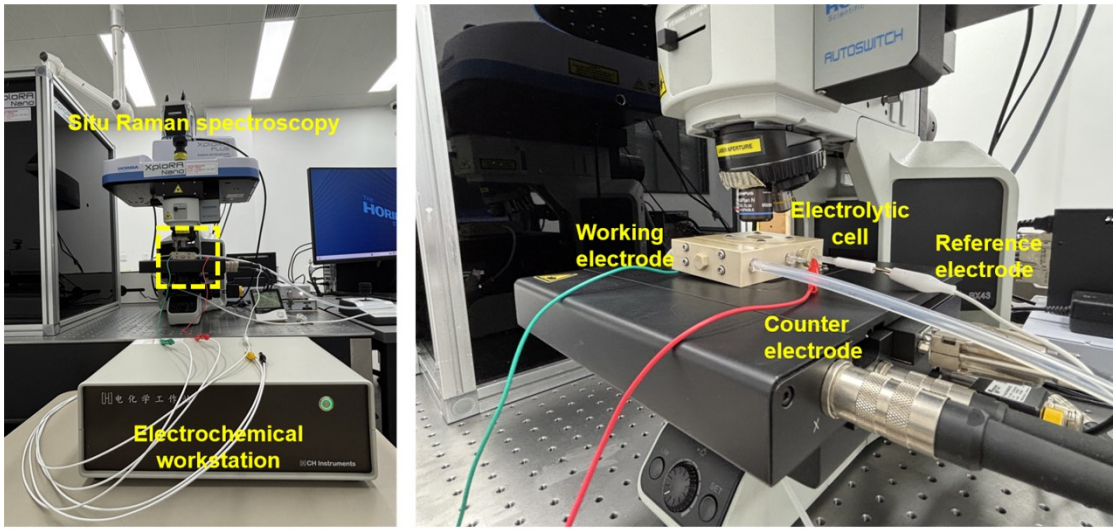

Fig. S20 The optical photograph of in-situ Raman measurement.

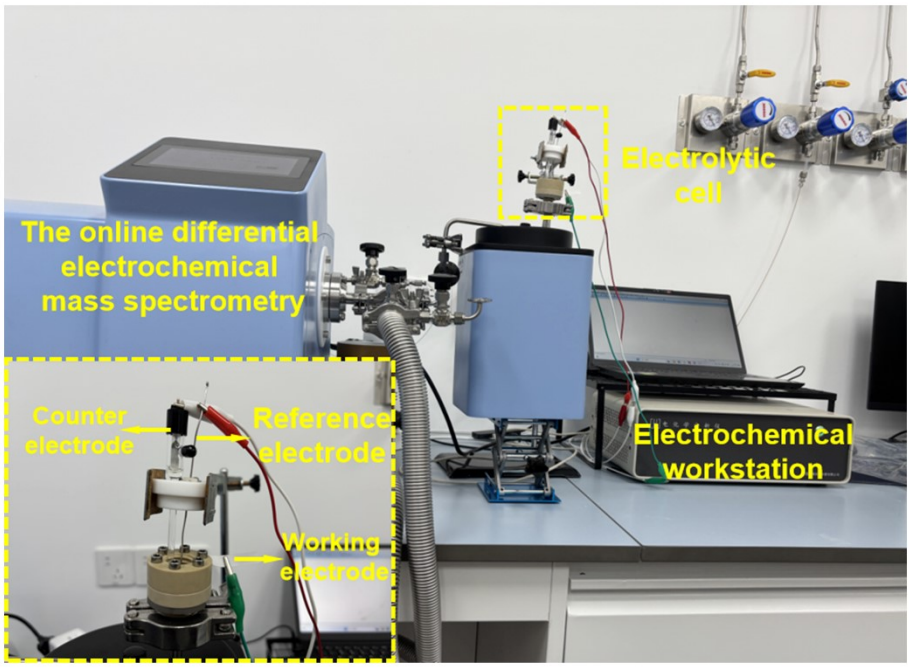

Fig. S21 The optical photograph of online DEMS measurement.

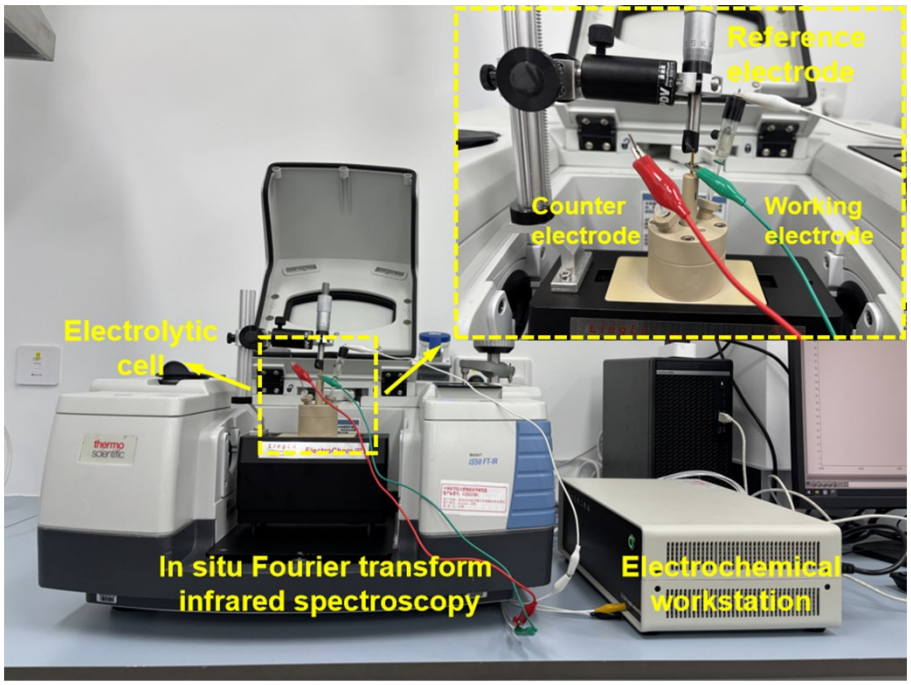

Fig. S22 The optical photograph of in-situ infrared (IR) measurement.

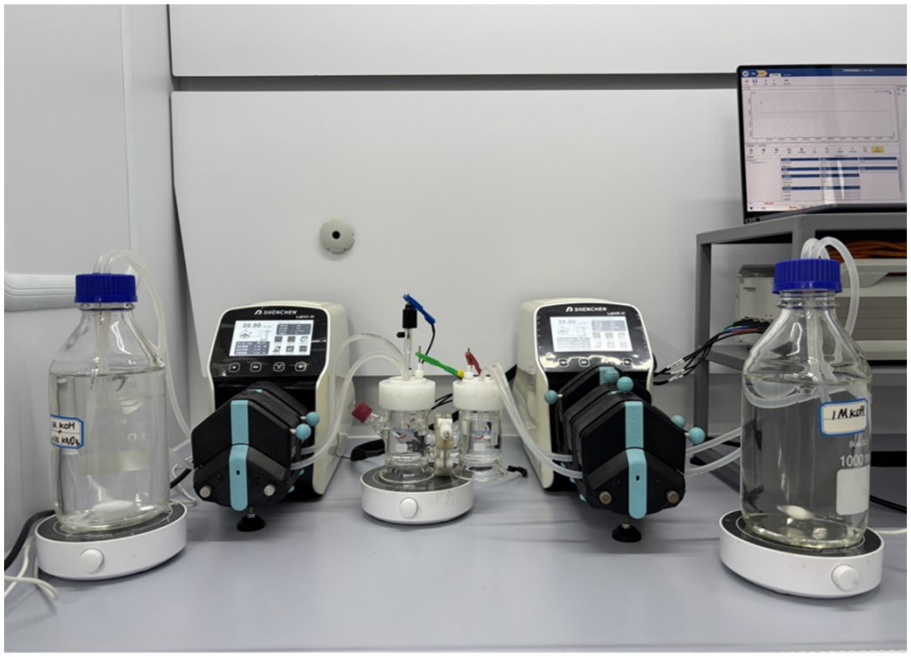

Fig. S23 Schematic illustration of the H-type electrochemical flow cell setup.

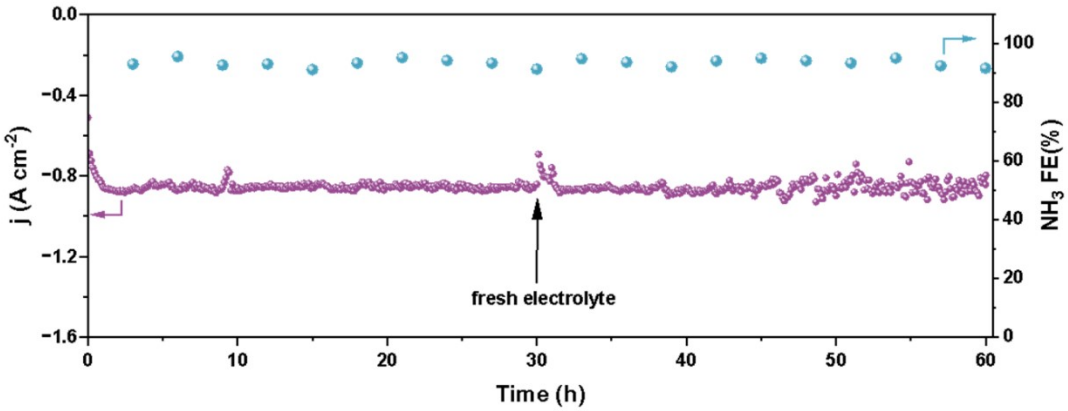

Fig. S24 Long-time test of CoMoP/NiCoP/NF at -0.4V (*vs.* RHE) in 1.0 M KOH + 0.1 M KNO_3 electrolyte.

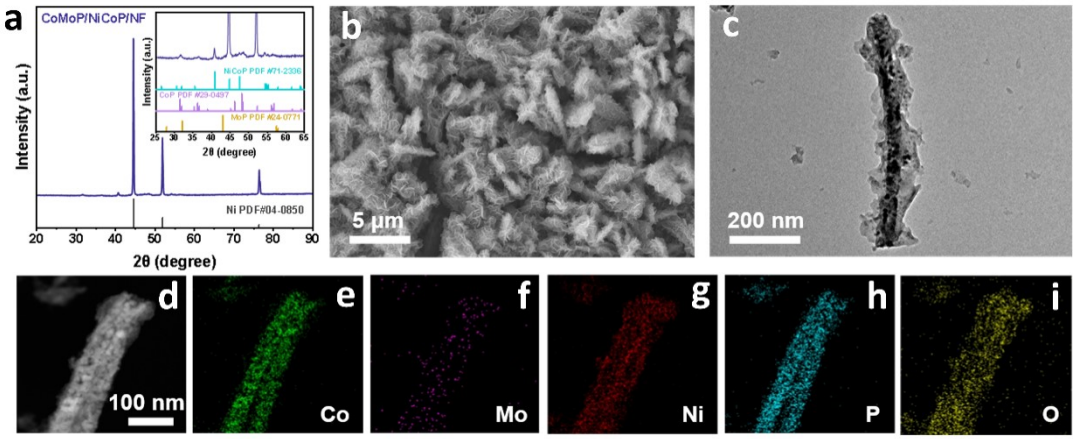

Fig. S25 (a) XRD pattern, (b) SEM image, (c) Low-magnification TEM image, (d-i) HAADF-STEM image and corresponding element mappings of CoMoP/NiCoP/NF after long-time eNO_3^-RR.

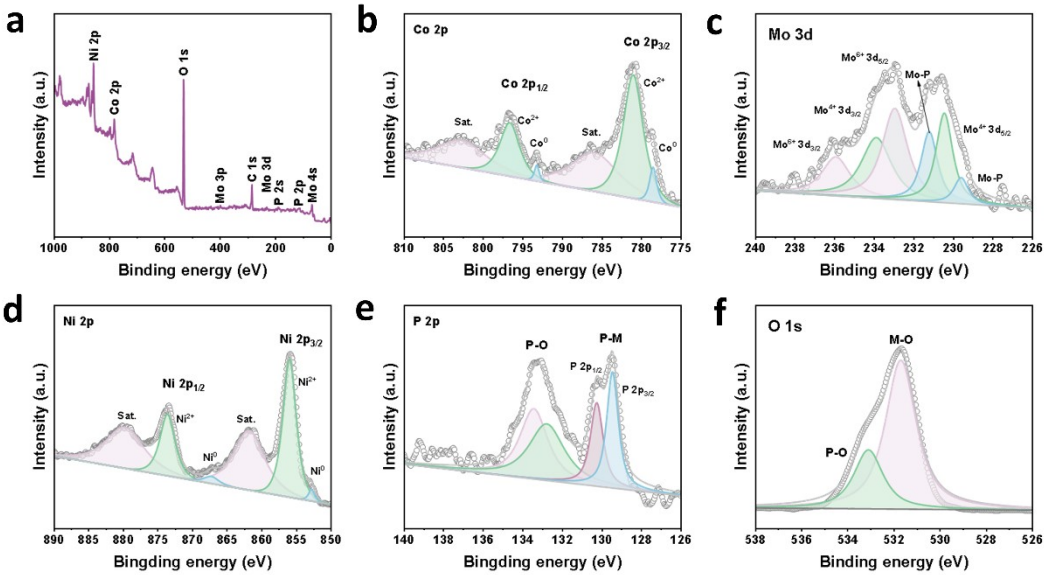

Fig. S26 (a) Surface survey XPS spectrum and high-resolution (b) Co 2p, (c) Mo 3d, (d) Ni 2p, (e) P 2p and (f) O 1s XPS spectra of CoMoP/NiCoP/NF after long-time eNO_3^-RR.

Table S1. NH3 yield rates (mg h^{-1} cm^{-2}) of various Catalyst at different applied potentials.

Potential (V *vs*. RHE)	**CoMoP/NiCoP/NF**	**NiCoP/NF**
0 V (*vs*. RHE)	9.92±0.83	5.00±0.13
-0.1 V (*vs*. RHE)	19.9±0.22	11.9±0.57
-0.2 V (*vs*. RHE)	31.8±0.74	22.5±1.39
-0.3 V (*vs*. RHE)	44.7±2.35	35.7±0.04
-0.4 V (*vs*. RHE)	61.8±1.13	47.0±1.09
-0.5 V (*vs*. RHE)	69.5±0.87	56.6±0.44
-0.6 V (*vs*. RHE)	77.8±0.74	63.2±0.74
-0.7 V (*vs*. RHE)	83.4±2.18	67.5±1.31
-0.8 V (*vs*. RHE)	88.6±3.04	68.9±1.61

Table S2. NH_3 FEs (%) of various Catalyst at different applied potentials.

Potential (V *vs*. RHE)	**CoMoP/NiCoP/NF**	**NiCoP/NF**
0 V (*vs*. RHE)	74.1±2.06	44.1±0.97
-0.1 V (*vs*. RHE)	83.0±1.70	55.9±1.00
-0.2 V (*vs*. RHE)	85.6±0.32	67.9±0.83
-0.3 V (*vs*. RHE)	92.4±0.69	78.2±0.45
-0.4 V (*vs*. RHE)	94.9±0.38	87.8±1.50
-0.5 V (*vs*. RHE)	90.9±0.63	83.8±0.86
-0.6 V (*vs*. RHE	88.8±0.72	82.1±0.59
-0.7 V (*vs*. RHE	85.1±1.34	80.1±1.91
-0.8 V (*vs*. RHE)	81.3±1.00	76.1±1.39

Table S3. NO_2^- FEs (%) of various Catalyst at different applied potentials.

Potential (V *vs*. RHE)	**CoMoP/NiCoP/NF**	**NiCoP/NF**
0 V (*vs*. RHE)	24.1±0.28	45.8±0.95
-0.1 V (*vs*. RHE)	16.0±1.00	28.0±1.03
-0.2 V (*vs*. RHE)	13.1±1.10	19.5±1.16
-0.3 V (*vs*. RHE)	4.71±0.27	12.3±0.35
-0.4 V (*vs*. RHE)	3.72±0.11	7.70±0.86
-0.5 V (*vs*. RHE)	1.34±0.12	2.46±0.44
-0.6 V (*vs*. RHE	0.52±0.04	1.65±0.09
-0.7 V (*vs*. RHE	0.32±0.04	0.92±0.16
-0.8 V (*vs*. RHE)	0.16±0.05	0.68±0.16

Table S4. NH3 yield rates (mg h^{-1} cm^{-2}) and NH_3 FEs (%) for different catalysts at -0.4 V (*vs.* RHE).

Catalyst	NH_3 yield rate (mg h^{-1} cm^{-2})	FE (%)
CoMoP/NiCoP/NF	61.8	94.9
NiCoP/NF	47.0	87.8
CoMoO/NiCoO/NF	7.8	49.9
NF	5.2	61.3

Table S5. The current density (A cm^{-2}) and the NH_3 partial current density at different potentials on CoMoP/NiCoP/NF.

Potential (V *vs*. RHE)	j_{Total}	j_{NH3}
0 V (*vs*. RHE)	-0.175	-0.130
-0.1 V (*vs*. RHE)	-0.296	-0.245
-0.2 V (*vs*. RHE)	-0.478	-0.409
-0.3 V (*vs*. RHE)	-0.636	-0.587
-0.4 V (*vs*. RHE)	-0.809	-0.768
-0.5 V (*vs*. RHE)	-0.951	-0.864
-0.6 V (*vs*. RHE	-1.103	-0.980
-0.7 V (*vs*. RHE	-1.200	-1.021
-0.8 V (*vs*. RHE)	-1.397	-1.135

Table S6. Comparison of relevant Energy consumptions (E_{spec}) (kWh kg^{-1}) for different catalysts at -0.4 V (*vs.* RHE).

Catalyst	**j_{NH3} (A cm^{-2})**	**NH_3 FE (%)**	**V_{cell} (V)**	**NH_3 Yield (mg h^{-1} cm^{-2})**	**(E_{spec}) (kWh kg^{-1})**
CoMoP/NiCoP/NF	-0.768	94.9	1.9	61.8	25.2
NiCoP/NF	-0.293	87.8	1.9	47.0	27.3
CoMoO/NiCoO/NF	-0.039	49.9%	1.9	7.8	47.7
NF	-0.026	61.3	1.9	5.2	39.1
Haber-Bosch Process	—	—	—	—	~30-40

Table S7. NH_3 yield rates (mg h^{-1} cm^{-2}) of CoMoP/NiCoP/NF at different concentrations.

Conditions	**Potential (V *vs*. RHE)**	**NH_3 yield rate (mg h^{-1} cm^{-2})**	**FE (%)**
1 M KOH + 0.025 M KNO_3	-0.4 V (*vs*. RHE)	24.6±0.30	72.8±2.38
1 M KOH + 0.05 M KNO_3	-0.4 V (*vs*. RHE)	44.6±0.03	93.7±0.31
1 M KOH + 0.1 M KNO_3	-0.4 V (*vs*. RHE)	61.8±1.13	94.9±0.38
1 M KOH + 0.25 M KNO_3	-0.4 V (*vs*. RHE)	78.3±0.38	86.7±1.67

Table S8. The charge-transfer resistance (R_{ct}) value of CoMoP/NiCoP/NF and NiCoP/NF under different conditions.

Catalyst	Conditions	R_{ct} ($\Omega \cdot cm^2$)
CoMoP/NiCoP/NF	1 M KOH + 0.1 M KNO_3	1.66
	1 M KOH	7.79
NiCoP/NF	1 M KOH + 0.1 M KNO_3	2.79
	1 M KOH	15.4

Table S9. The comparison results of our work with previously reported eNO_3^-RR works on NH_3 yield performance.

Catalyst	Conditions	Potential (V *vs.* RHE)	NH_3 yield rate	FE (%)	Ref.
CoMoP/NiCoP/NF	**1 M KOH + 0.1 M KNO_3**	**-0.4**	**61.8 mg h^{-1} cm^{-2}**	**94.9**	**This work**
CuCoSP	0.1 M KOH + 0.1 M KNO_3	-0.175	19.89 mg h^{-1} cm^{-2}	90.6	2
Fe/Ni_2P	0.2 M KSO_4 + 0.05 M KNO_3	-0.4	4.17 mg h^{-1} cm^{-2}	94.3	3
Fe-SAC	1 M KOH + 0.1 M KNO_3	-0.21	10.2 mg h^{-1} cm^{-2}	86	4
Bi_2S_3/MoS_2/CC	0.1 M Na_2SO_4 + 0.1 M $NaNO_3$	-0.8	2.55 mg h^{-1} cm^{-2}	88.4	5
Ni-MoS_2	1 M KOH + 0.1 M KNO_3	-0.3	4.76 mg h^{-1} cm^{-2}	92.3	6
Pd@Cu	1 M KOH + 0.1 M KNO_3	-0.4	13.1 mg h^{-1} cm^{-2}	92.5	7
o-CoP/C@ Cu_3P	1 M KOH + 0.1 M KNO_3	-0.25	26.8 mg h^{-1} cm^{-2}	90.27	8
CuNi-LDHs	0.1 M KOH + 0.1 M KNO_3	-0.4	2.73 mg h^{-1} cm^{-2}	94.65	9
RuCu DAs/NGA	0.1 M KOH + 0.1 M KNO_3	-0.4	3.10 mg h^{-1} cm^{-2}	95.7	10
Cu_3P NA/CF	0.1 M PBS + 0.1 M KNO_2	-0.5	1.63 mg h^{-1} cm^{-2}	91.2	11
FeMo-DSAC	1 M KOH + 0.1 M KNO_3	-0.78	13.56 mg h^{-1} cm^{-2}	~81	12
CoP-CNS	1 M KOH + 1 M KNO_3	-1.03	52.58 mg h^{-1} cm^{-2}	90.5	13
Cu5/$Mo_{0.6}$-WO_3	0.1 M KOH + 0.1 M KNO_3	-0.7	5.25 mg h^{-1} cm^{-2}	98.6	14
CoP/Cu_3P	0.1 M KOH + 0.1 M KNO_3	-0.3	27.03 mg h^{-1} cm^{-2}	96.4	15
FeMo-N-C	0.05 M PBS + 0.16 M NO_3^-	-0.45	0.3 mg h^{-1} cm^{-2}	94.7	16
1T-MoS_2	0.5 M Na_2SO_4 + 0.01 M $NaNO_3$	-0.5	0.34 mg h^{-1} cm^{-2}	88.12	17

Reference

1 Y. Li, Y. Liu, M. Zhang, L. Li, Z. Jiang, B. Han, B. Wang and J. Li, *Angew. Chem., Int. Ed.*, 2025, **64**, e202417631.

2 W. He, J. Zhang, S. Dieckhöfer, S. Varhade, A. C. Brix, A. Lielpetere, S. Seisel, J. R. C. Junqueira and W. Schuhmann, *Nat. Commun.*, 2022, **13**, 1129.

3 W. Yang, Z. Chang, X. Yu, R. Shen, L. Wang, X. Cui and J. Shi, *Angew. Chem., Int. Ed.*, 2025, **64**, e202415300.

4 Z.-Y. Wu, M. Karamad, X. Yong, Q. Huang, D. A. Cullen, P. Zhu, C. Xia, Q. Xiao, M. Shakouri, F.-Y. Chen, J. Y. Kim, Y. Xia, K. Heck, Y. Hu, M. S. Wong, Q. Li, I. Gates, S. Siahrostami and H. Wang, *Nat. Commun.*, 2021, **12**, 2870.

5 X. Liu, X. Xu, F. Li, J. Xu, H. Ma, X. Sun, D. Wu, C. Zhang, X. Ren and Q. Wei, *ACS Appl. Mater. Interfaces*, 2022, **14**, 38835–38843.

6 J. Lv, X. Sun, F. Wang, R. Yang, T. Zhang, T. Liang, W. Rong, Q. Yang, W. Xue, L. Wang, X. Xu and Y. Liu, *Adv. Funct. Mater.*, 2024, **34**, 2411491.

7 S. K. Anbarasu, J. Cherusseri, R. A. Senthil, A. Kumar, M. Ubaidullah and M. Y. Choi, *Appl. Catal., B: Environ Energy*, 2026, **383**, 126103.

8 Y. Li, Z. Lu, L. Zheng, X. Yan, J. Xie, Z. Yu, S. Zhang, F. Jiang and H. Chen, *Energy Environ. Sci.*, 2024, **17**, 4582–4593.

9 H. Li, S. Li, R. Guan, Z. Jin, D. Xiao, Y. Guo and P. Li, *ACS Catal.*, 2024, **14**, 12042–12050.

10 K. Liu, Z. Sun, X. Peng, X. Liu, X. Zhang, B. Zhou, K. Yu, Z. Chen, Q. Zhou, F. Zhang, Y. Wang, X. Gao, W. Chen and P. Chen, *Nat. Commun.*, 2025, **16**, 2167.

11 J. Liang, B. Deng, Q. Liu, G. Wen, Q. Liu, T. Li, Y. Luo, A. A. Alshehri, K. A. Alzahrani, D. Ma and X. Sun, *Green Chem.*, 2021, **23**, 5487–5493.

12 J. Wan, H. Zhang, J. Yang, J. Zheng, Z. Han, W. Yuan, B. Lan and X. Li, *Appl. Catal., B: Environ Energy*, 2024, **347**, 123816.

13 K. Fan, W. Xie, J. Li, Y. Sun, P. Xu, Y. Tang, Z. Li and M. Shao, *Nat. Commun.*, 2022, **13**, 7958.

14 Y. Dai, S. Li, X. Li, K. Liu, Y. Guo, H. Li and B. Jiang, *Adv. Funct. Mater.*, 2025, **35**, 2420282.

15 H. Xu, J. Peng, P. Li, X. Feng, J. Hu, G. Han, J. Xu, D. Wang, Z. Lu, G. Li and J. Yang, *Angew. Chem., Int. Ed.*, 2025, e22410.

16 E. Murphy, Y. Liu, I. Matanovic, S. Guo, P. Tieu, Y. Huang, A. Ly, S. Das, I. Zenyuk, X. Pan, E. Spoerke and P. Atanassov, *ACS Catal.*, 2022, **12**, 6651–6662.

17 G. Lin, Q. Ju, X. Guo, W. Zhao, S. Adimi, J. Ye, Q. Bi, J. Wang, M. Yang and F. Huang, *Adv. Mater.*, 2021, **33**, 2007509.